Journal of Power Sources 195 (2010) 5278–5291

Contents lists available at ScienceDirect

Journal of Power Sources

journal homepage: www.elsevier.com/locate/jpowsour

A numerical investigation on multi-phase transport phenomena in a proton exchange membrane fuel cell stack

Anh Dinh Le, Biao Zhou*

Department of Mechanical, Automotive & Materials Engineering, University of Windsor, 401 Sunset Ave., Windsor, ON, Canada N9B 3P4

ARTICLE INFO

Article history:
Received 3 February 2010
Received in revised form 4 March 2010
Accepted 4 March 2010
Available online 16 March 2010

Keywords:
PEMFC
Stack
VOF
CFD
Liquid water
Multi-phase

ABSTRACT

In this study, the simulation of a fuel cell stack is performed by applying a general numerical model with VOF method that has been successfully applied to single PEMFC model to investigate the fluid dynamics, mass transport, flooding phenomenon and the effects of liquid water on the stack performance. The performance of three single cells in series connection in the fuel cell stack is examined according to the presence of liquid water in different single cells. The distributions of fluid flow, species concentration and the current density are presented to illustrate the effects of liquid water on the performance of each single cell. The numerical results locate that the low distributions of species in the flooding cell certainly degrade the performance of this cell. Moreover, it can be seen that the performance of the flooding cell will significantly affect the whole stack performance since the values of average current density must be identical in all single cells.

1. Introduction

A proton exchange membrane fuel cell (PEMFC), an electrochemical conversion device, with its prominent advantages comprising of simplicity, quick start-up, fast response to charge of load, high efficiency and power density, no moving parts, low operating temperature, reduced corrosion problems and especially zero emissions; is one of the most promising solutions for alternative energy sources in the near future.

A single PEM fuel cell has a simple structure. It usually has two electrodes: anode and cathode and a membrane electrolyte. Hydrogen is oxidized in the anode and oxygen is reduced in the cathode. Protons are transported from the anode to the cathode through the polymer electrolyte membrane (or proton exchange membrane—PEM) and electrons are carried to the cathode from the anode over an external circuit (electric load). In the cathode, oxygen reacts with protons and electrons, forming by-product water and generating heat. However, the theoretical potential of a single PEMFC is approximately 1 V and its practical potential is smaller than 1 V. To generate more current and voltage that are required for industrial and transportation applications, single fuel cells are stacked in practice. By having multiple cells connected in series and/or parallel, the voltage and/or current of a stack will be multiplied, generating the required high power output. However, connecting single cells into a fuel cell stack leads to an increase in size and weight of the fuel cell, resulting in important issues in stack design such as: the distribution of reactant gas flow through the channels of the single cells and by-products water exhaust through the manifold, heat transfer and removal, water management of the stack, etc. These issues have been critical challenges in PEM fuel cell stack design and optimization. Modeling a single fuel cell with a small size and simple geometry is more straightforward than modeling a complete fuel cell stack. Until now, many scientists have focused on unsteady, single- or multi-phase, one-, two- or three-dimensional models of the single cell as discussed in prominent studies [1–15]. These researchers have significantly contributed to single PEMFC research and development.

Contrary to the large number of researches on the single PEMFC model that have been developed as mentioned above, few studies focusing on the modeling of fuel cell stack have been introduced so far. Modeling a fuel cell stack with a complex geometry at adequate grid solution and calculation time is still a big challenge. On the other hand, a large number in such these studies nearly focuses on investigation of dynamic response and dynamic behaviors of PEMFCs. The models that consider simulations on physical and electrochemical phenomena and flow field, heat and mass transports characteristics of a PEMFC have been rarely discussed. Shan et al. [16] have setup a 2D PEMFC stack model that examines the fluid and thermal characteristic, especially focusing on temperature transport. Species, heat and charge transports in a mini PEMFC stack were also reported in a study of Liu et al. [17]. Numerical investigations on pressure and velocity distribution in the manifold of a

* Corresponding author. Tel.: +1 519 253 3000x2630; fax: +1 519 973 7007.
E-mail address: bzhou@uwindsor.ca (B. Zhou).

0378-7753/$ – see front matter.
doi:10.1016/j.jpowsour.2010.03.014

Nomenclature

a	water activity
A_{surf}	reactive surface area (m^2)
A_s	heat transfer surface area (m^2)
c_p	specific heat capacity ($J\,kg^{-1}\,K^{-1}$)
C_i	species concentration i ($kmol\,m^{-3}$)
D_i	diffusion coefficient of species i in gas mixture ($m^2\,s^{-1}$)
F	Faraday constant ($9.6487 \times 10^7\,C\,kmol^{-1}$)
h	convective heat transfer ($W\,m^{-2}\,K^{-1}$)
h_L	the enthalpy of formation of water vapor ($N\,m\,kg^{-1}$)
I	current density ($A\,m^{-2}$)
$\bar{I}$	total current (A)
J	mass flux ($kg\,m^{-2}\,s^{-1}$)
k_{eff}	effective thermal conductivity ($W\,m^{-1}\,K^{-1}$)
M_i	molecular weight of species i in gas mixture ($kg\,kmol^{-1}$)
n_d	electro-osmotic drag coefficient
n_f	charge number of the sulfonic acid ion
P	pressure (Pa)
P_i	partial pressure of species i (Pa)
$\dot{Q}$	heat rate (W)
R	volumetric current density ($A\,m^{-3}$)
S	source term
t	time (s)
T	temperature (K)
u, v, w	velocities in x, y, and z directions, respectively ($m\,s^{-1}$)
V_{oc}	open-circuit potential (V)
V_{cell}	cell potential (V)
~~V~~	volume (m^3)
X_i	mole fraction of species i
Y_i	mass fraction of species i

Greek symbols

α	transfer coefficient
β	the factor accounts for energy release
ε	porosity
ϕ	phase potential (V)
γ	concentration dependence
γ_p, γ_T	exponent factors
η	overpotential (V)
φ	relative water content
κ	surface curvature
τ_g	gaseous permeability (m^2)
τ_l	liquid permeability (m^2)
τ_p	hydraulic permeability (m^2)
τ_ϕ	electrokinetic permeability (m^2)
λ	water content
μ	dynamic viscosity ($kg\,m^{-2}\,s^{-1}$)
ρ	density of gas mixture ($kg\,m^{-3}$)
ρ_i	density of species i ($kg\,m^{-3}$)
σ	phase conductivity ($\Omega^{-1}\,m^{-1}$)
υ	reaction rate ($kmol\,m^2\,s^{-1}$)
ω	excess coefficient
χ	surface tension coefficient ($N\,m^{-1}$)
θ_w	contact angle (°)

Subscripts and superscripts

an	anode
cat	cathode
cond	condensation
e	electrochemical reaction
eff	effective
evap	evaporation
g	gas phase
i	species *i*
in	inlet
l	liquid phase
m	membrane phase
out	outlet
ref	reference
s	solid phase
sat	saturated
w	water vapor

fuel cell stack have been developed by Chen et al. [18], Mustata et al. [19]. In another study, a detailed numerical analysis of the transport and electrochemical phenomena involved in a fuel cell stack operation has been presented by Pitchumani and co-workers [20]. A complete three-dimensional CFD model has been developed to predict how the baseline operation and original design of the stack impact the local temperature, water content, water transport, and kinetic variables inside the individual cells of the stack by Shimpalee et al. [21]. Liquid water transport and its effects on airflow in a PEMFC stack were firstly presented by Zhou and co-workers [22]. The results showed that there were significant variations of water distribution and pressure drop in different cells at different times. Recently, two-phase flow modeling has been applied to a fuel cell stack [23] to predict the stack performance and flooding phenomenon under various operating conditions.

In this present study, we apply our general PEMFC model previously that is used for single PEFMCs [13,15] into a PEMFC stack. The general model is a 3D, unsteady, multi-phase numerical model with all detailed physics including fluid dynamics, multi-components transport, heat transfer, phase change and electrochemical reactions coupled with volume-of-fluid (VOF) gas–liquid interface tracking. The advantages of the model are that it can investigate the liquid water transport and predict the presence of liquid water and flooding phenomenon in the channels and porous media of a fuel cell stack. The numerical results of the cases with and without the presence of liquid water illustrate how liquid drops affect physical and transport characteristics of each single cell in the stack and how the change on the performance of each single cell influences the overall stack performance.

2. Description of mathematical model

2.1. The stack geometry and model assumptions

The fuel cell stack model comprises of three single PEMFCs connected in series with a parallel-designed channel used in each single cell as shown in Fig. 1. The width and height of the channels are identical and are 1 mm. The channel inlets and outlets of the three single cells are connected to the gas inlets and outlets by the manifolds. The fuel cell stack includes current collectors, middle bipolar plates, flow channels, gas diffusion layers (GDLs), catalyst layers, proton exchange membranes and manifolds. There are main assumptions of the model described as follows:

1. The fluid flow in the fuel cell was laminar due to the low flow velocities and the small size of gas flow channels and manifolds.
2. The porous media including membrane, catalyst layers and GDLs were considered to be isotropic in all single cells.
3. There are no cooling channels used for each single cell. The fuel cell cooling is controlled by forced convection heat transfer applied on the outside surfaces of the stack.

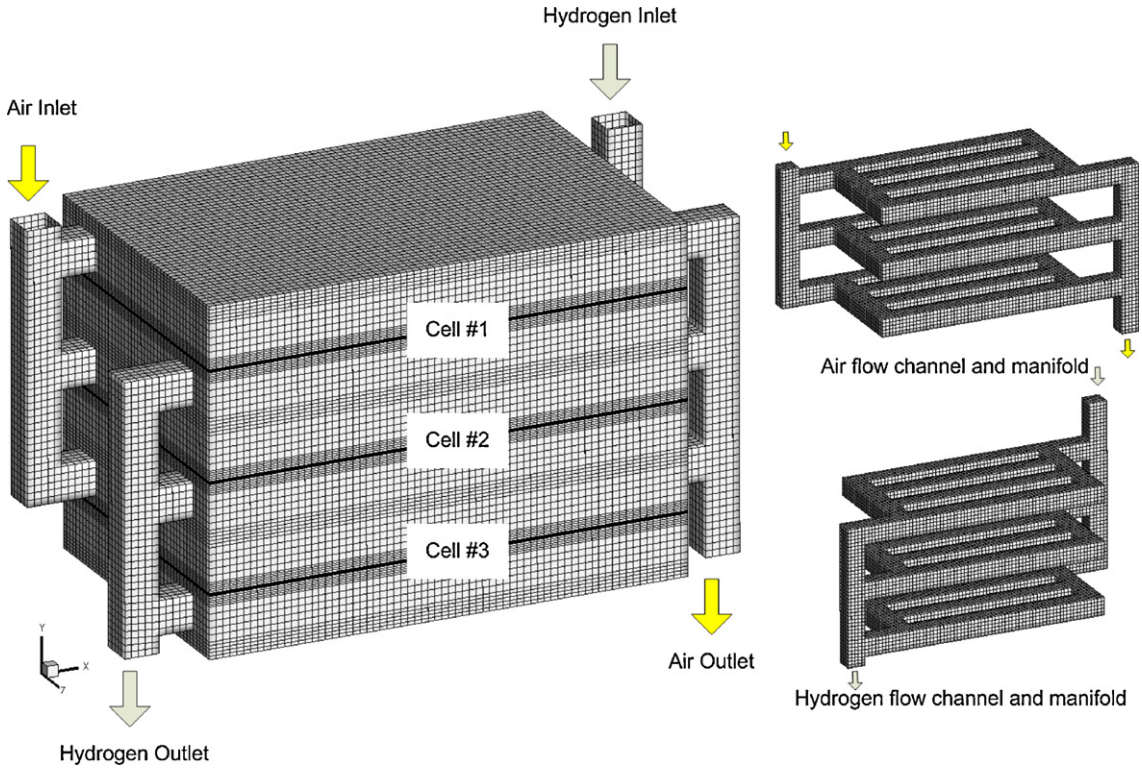

Fig. 1. Schematic diagram and computational domain of the fuel cell stack.

2.2. Mathematical equations

Similar to single PEMFC modeling, the PEMFC stack modeling is governed by principal conservation equations: mass and momentum for solving fluid flow, energy for solving heat generation and transfer, species for solving species transport, and charge for solving current density and voltage distribution. Furthermore, to track gas–liquid interface in liquid transport, the volume fraction equation is also coupled.

Mass and momentum conservations in the fuel cell are presented by continuity equation (1), volume fraction equation (2) and momentum equation (3), as follows:

$$\frac{\partial \varepsilon\rho}{\partial t} + \nabla\cdot(\varepsilon\rho\vec{v}) = S_m \tag{1}$$

$$\frac{\partial}{\partial t}(\varepsilon s_l\rho_l) + \nabla(\varepsilon s_l\rho_l\vec{v}_l) = S_l \tag{2}$$

$$\frac{\partial}{\partial t}(\varepsilon\rho\vec{v}) + \nabla(\varepsilon\rho\vec{v}\vec{v}) = -\varepsilon\nabla p + \nabla[\varepsilon\mu\nabla\vec{v}] + S_v \tag{3}$$

The velocity and density of flow mixture including gas and liquid phases are considered as the variables in these equations. The relation between mixture density and phases' densities is given as:

$$\rho = s_l\rho_l + (1-s_l)\rho_g \tag{4}$$

The tracking of the interface between the phases is accomplished by the solution of a continuity equation for the volume fraction of one of the phases for two-phase model using VOF method. The interface tracking between gas and liquid of different density and viscosity are defined by volume fraction of liquid water s_l and volume fraction of the gaseous phase s_g [24]. Eq. (2) is employed to track the volume fluid of liquid phase and it is solved for entire domain. The volume fraction of the gas phase is automatically computed based on the relative equation:

$$s_l + s_g = 1 \tag{5}$$

The source term of Eq. (2) is the source of liquid water as the liquid water is formed by phase change process in the fuel cell.

A single momentum equation is solved throughout the domain and the resulting velocity field is shared between gas and liquid phases [23]. The momentum equation (3) is dependent on the volume fractions of gas and liquid phases through the mixture properties:

$$\mu = s_l\mu_l + (1-s_l)\mu_g \tag{6}$$

The source terms for the mass, volume fraction and momentum equations for different layers of the PEMFC are listed in Table 1. The mass source term is available only for the anode and cathode catalyst layers where the mass generation and consumption are present. For the momentum equation, the gravity effect is taken into consideration in the momentum source terms. In different layers of the porous media, the other source terms are added to describe the flow of the fluid through a porous zone by using viscous loss—Darcy's drag force.

The energy equation accounting for unsteady, two-phase flow is shown as below:

$$(\rho c_p)_{eff}\frac{\partial T}{\partial t} + (\rho c_p)_{eff}(\vec{v}\nabla T) = \nabla\left(k_{eff}\nabla T - \sum_j h_j\vec{J}_j + (\tau\cdot\vec{v})\right) + S_T \tag{7}$$

Since energy and mixture thermal properties of two-phase are also shared between gas and liquid phases [23]:

$$(\rho c_p)_{eff} = \varepsilon\rho_f c_{p,f} + (1-\varepsilon)\rho_s c_{p,s} \tag{8}$$

$$k_{eff} = \varepsilon k_s + (1-\varepsilon)k_f \tag{9}$$

The first three terms in the right-hand side of Eq. (7) represent energy transfer due to heat conduction in both solid and fluid

Table 1
The source terms of governing equations.

Governing equation	Volumetric source terms and location of application
Conservation of mass	For gas channels, GDL and the membrane $S_m = 0$ For anode catalyst layer: $S_m = -\frac{M_{H_2}}{2F} R_{an}$ For cathode catalyst layer: $S_m = -\frac{M_{O_2}}{4F} R_{cat} + \frac{M_{H_2O}}{2F} R_{cat}$
Volume fraction	For all parts: $S_s = r_w$
Conservation of momentum	For gas channels: $S_v = \rho\vec{g}$ For GDLs and void of catalyst layers: $S_v = \rho\vec{g} - \frac{\mu}{\tau_g}\varepsilon^2\vec{v} + \chi\kappa\frac{2\rho\nabla s_l}{(\rho_l+\rho_g)}$ For membrane: $S_v = \rho\vec{g} - \frac{\mu}{\tau_g}\varepsilon^2\vec{v} + \chi\kappa\frac{2\rho\nabla s_l}{(\rho_l+\rho_g)} + \frac{\tau_\phi}{\tau_p} c_f n_f F \nabla\phi_m$
Conservation of energy	For current collectors: $S_T = \frac{I^2}{\sigma_s}$ For gas flow channel: $S_T = r_w h_L$ For GDL: $S_T = \frac{I^2}{\sigma_s^{eff}} + r_w h_L$ For membrane: $S_T = \frac{I^2}{\sigma_m^{eff}} + r_w h_L$ For catalyst layer: $S_T = \eta R_{an,cat} + I^2\left(\frac{1}{\sigma_s^{eff}} + \frac{1}{\sigma_m^{eff}}\right) + r_w h_L$
Hydrogen transport	For anode catalyst layer: $S_{H_2} = -\frac{M_{H_2}}{2F} R_{an}$
Oxygen transport	For cathode catalyst layer: $S_{O_2} = -\frac{M_{O_2}}{4F} R_{cat}$
Water vapor transport	For anode catalyst layer: $S_{H_2O} = \left(\frac{n_d M_{H_2O}}{F}\right)\nabla I_m - r_w$ For cathode catalyst layer: $S_{H_2O} = \frac{M_{H_2O}}{2F} R_{cat} + \left(\frac{n_d M_{H_2O}}{F}\right)\nabla I_m - r_w$ For the membrane $S_{H_2O} = \left(\frac{n_d M_{H_2O}}{F}\right)\nabla\vec{I}_m - r_w$
Conservation of charge	For anode catalyst layer: $S_{es} = -R_{an}, \quad S_{em} = R_{an}$ For cathode catalyst layer: $S_{es} = R_{cat}, \quad S_{em} = -R_{cat}$ For other parts: $S_{es} = 0, \quad S_{em} = 0$

zones, heat diffusion, and heat source caused by viscous dissipation, respectively. In addition, other source terms are considered to be the heat from chemical reactions (only in the catalyst layers), Ohmic heat due to electric resistance of solid zones, and the heat due to phase change processes (condensation and evaporation). All the sources terms of energy equation in different layers are listed in detail in Table 1.

The conservation equations for species transport are solved in the two-phase flow by taking into account hydrogen, oxygen, water and nitrogen in gas mixture:

$$\frac{\partial}{\partial t}(\varepsilon\rho Y_h) + \nabla\cdot(\varepsilon\rho\vec{v}Y_h) = D_{h,m}\nabla^2(\rho Y_h) + S_h \tag{10}$$

$$\frac{\partial}{\partial t}(\varepsilon\rho Y_o) + \nabla\cdot(\varepsilon\rho\vec{v}Y_o) = D_{o,m}\nabla^2(\rho Y_o) + S_o \tag{11}$$

$$\frac{\partial}{\partial t}(\varepsilon\rho Y_{wv}) + \nabla\cdot(\varepsilon\rho\vec{v}Y_{wv}) = D_{wv,m}\nabla^2(\rho Y_{wv}) + S_{wv} \tag{12}$$

In this two-phase flow model, homogeneous gas phase chemical reactions are treated the same as a single-phase chemical reaction [24]. The reactants consumed and the products generated from the reactions are considered in the gas mixture. Based on solving the equations, it predicts the local mass fraction of each species, Y_i, through the solution of a convection-diffusion equation for the ith species, and $D_{i,m}$ is the diffusion coefficient for species i in the gas mixture defined as [25]:

$$D_{i,m} = \varepsilon^{1.5}(1-s_l)^{r_s} D_{i,m}^0 \left(\frac{P_0}{P}\right)^{\gamma_P}\left(\frac{T}{T_0}\right)^{\gamma_T} \tag{13}$$

where $D_{i,m}^0$ is the diffusion coefficient for species i in the mixture at the reference temperature and pressure. Since the mass

Table 2
Geometrical properties and physical parameters of the fuel cell stack model.

Parameters	Value
Anode channel width	0.001 m
Anode channel height	0.001 m
Cathode channel width	0.001 m
Cathode channel height	0.001 m
Manifolds width	0.001 m
Manifold height	0.001 m
Membrane thickness, δ_{mem}	50×10^{-6} m
GDL thickness, δ_{GDL}	300×10^{-6} m
Catalyst layer thickness, δ_{ct}	20×10^{-6} m
Active surface area, A_{surf} (per one single cell)	1.26×10^{-4} m^2
Number of single fuel cell in stack	3
Stack height, Y-coordinate	1.007×10^{-2} m
Stack length, X-coordinate	1.6×10^{-2} m
Stack width, Z-coordinate	0.9×10^{-2} m
Anode inlet excess coefficient, ω_a	4
Cathode inlet excess coefficient, ω_c	1.25
Operating voltage, V_{cell}	1.8 V
Anode inlet temperature, $T_{in,an}$	300 K
Cathode inlet temperature, $T_{in,cat}$	300 K
Anode volumetric reference exchange current density/reference hydrogen concentration, $R_{an}^{ref}/(C_{H_2}^{ref})^{\gamma_{an}}$	7×10^{10} A kmol^{-1}
Cathode volumetric reference exchange current density/reference oxygen concentration, $R_{cat}^{ref}/(C_{O_2}^{ref})^{\gamma_{cat}}$	7×10^{5} A kmol^{-1}
Anode transfer coefficient, α_{an}	0.5
Cathode transfer coefficient, α_{cat}	0.5
Anode concentration dependence, γ_{an}	0.5
Cathode concentration dependence, γ_{cat}	1.0
Factor accounts for energy release, β	0.5
Membrane porosity, ε_{mem}	0.5
Diffusion layer porosity, ε_{gdl}	0.5
Catalyst layer porosity, ε_{ct}	0.5
Permeability of porous media, τ	1.76×10^{-11} m^2
Contact angle of the channel, θ_w	70°
Surface tension, χ	0.065 N m^{-1}
Condensation rate, c_r	100 s^{-1}

Table 3
Three different cases of different droplet locations.

Case No.	Location of droplets	Number of droplets	Time of addition (s)
1	Cell #1—cathode channel	12	At 1 s
2	Cell #2—cathode channel	12	At 1 s
3	Cell #3—cathode channel	12	At 1 s

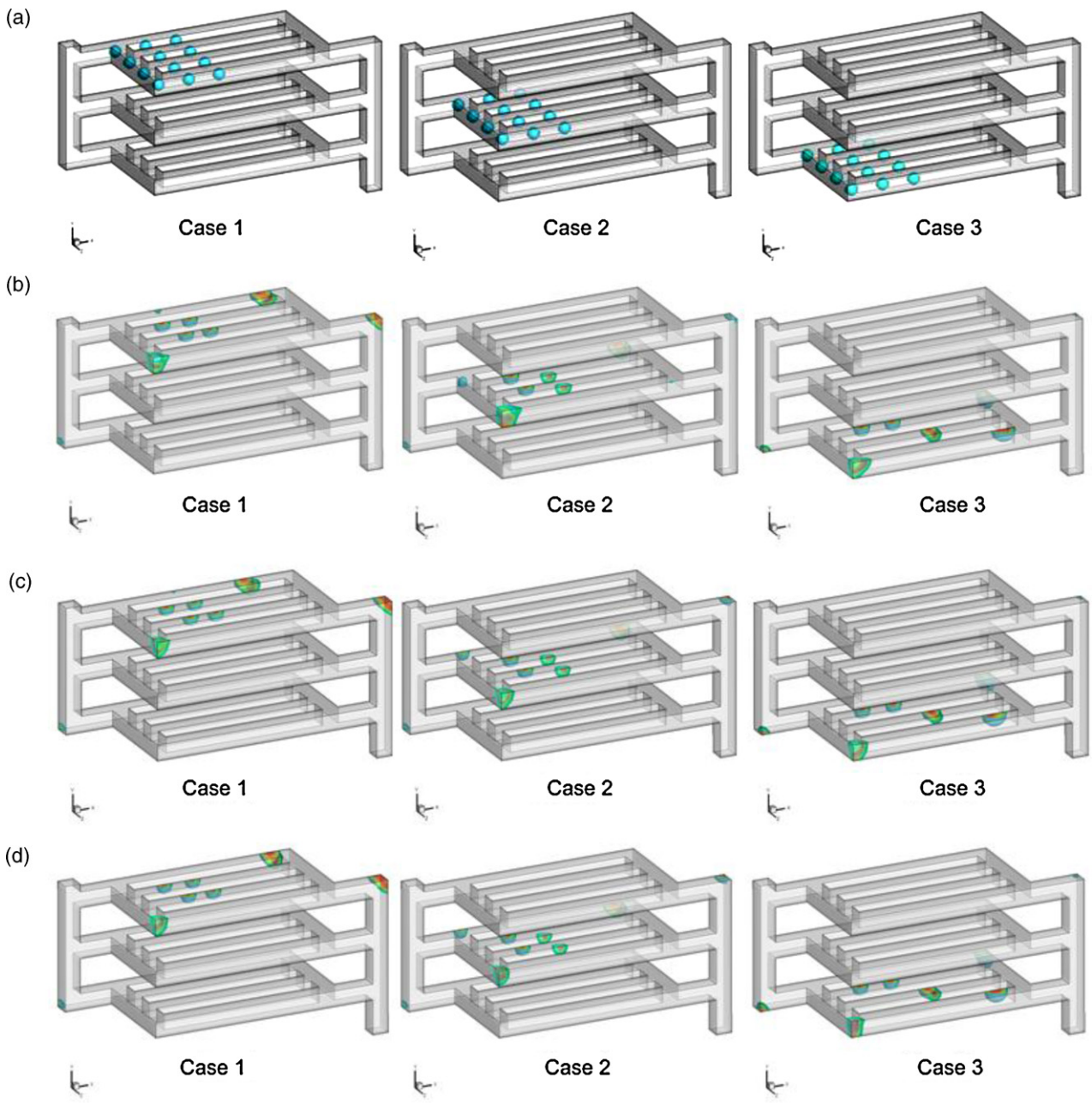

Fig. 2. Three different cases for different locations of droplet at (a) $t = 1$ s, (b) $t = 2$ s, (c) $t = 3$ s, and (d) $t = 4$ s.

fraction of the species sums to unity, the nitrogen mass fraction is determined as one minus the sum of the three solved mass fractions.

The source terms for hydrogen, oxygen and water transport in the anode and cathode catalyst layers are various and dependent on the transfer current generated by electrochemical reactions. While the hydrogen and oxygen are always consumed in the anode and cathode sides, respectively, then the by-product water in terms of vapor is generated in the cathode. Moreover, the protons move from the anode to the cathode also pull water molecules with their movement what is called the electro-osmotic drag effect. The water transport rate through the Nafion membrane from the anode to the cathode by the electro-osmotic drag is presented as a function of volumetric current density and the drag coefficient that were proposed by Springer et al. [2]. In Springer's formulations, the drag coefficient is defined to be a function of the water content inside the polymer membrane:

$$n_d = \frac{2.5}{22}\lambda \tag{14}$$

where the water content in the polymer electrolyte is related to water activity by using empirical equation [24]:

$$\lambda = \begin{cases} 0.043 + 17.18a - 39.85a^2 + 36a^3 & (0 \le a \le 1) \\ 14 + 1.4(a-1) & (1 \le a \le 3) \\ 16.8 & (a > 3) \end{cases} \tag{15}$$

In Eq. (16), the water activity is defined as a function of water vapor pressure, saturated pressure and liquid volume fraction in following form [24]:

$$a = \frac{P_w}{P_{sat}} = \frac{X_w P}{P_{sat}} + 2s_l \tag{16}$$

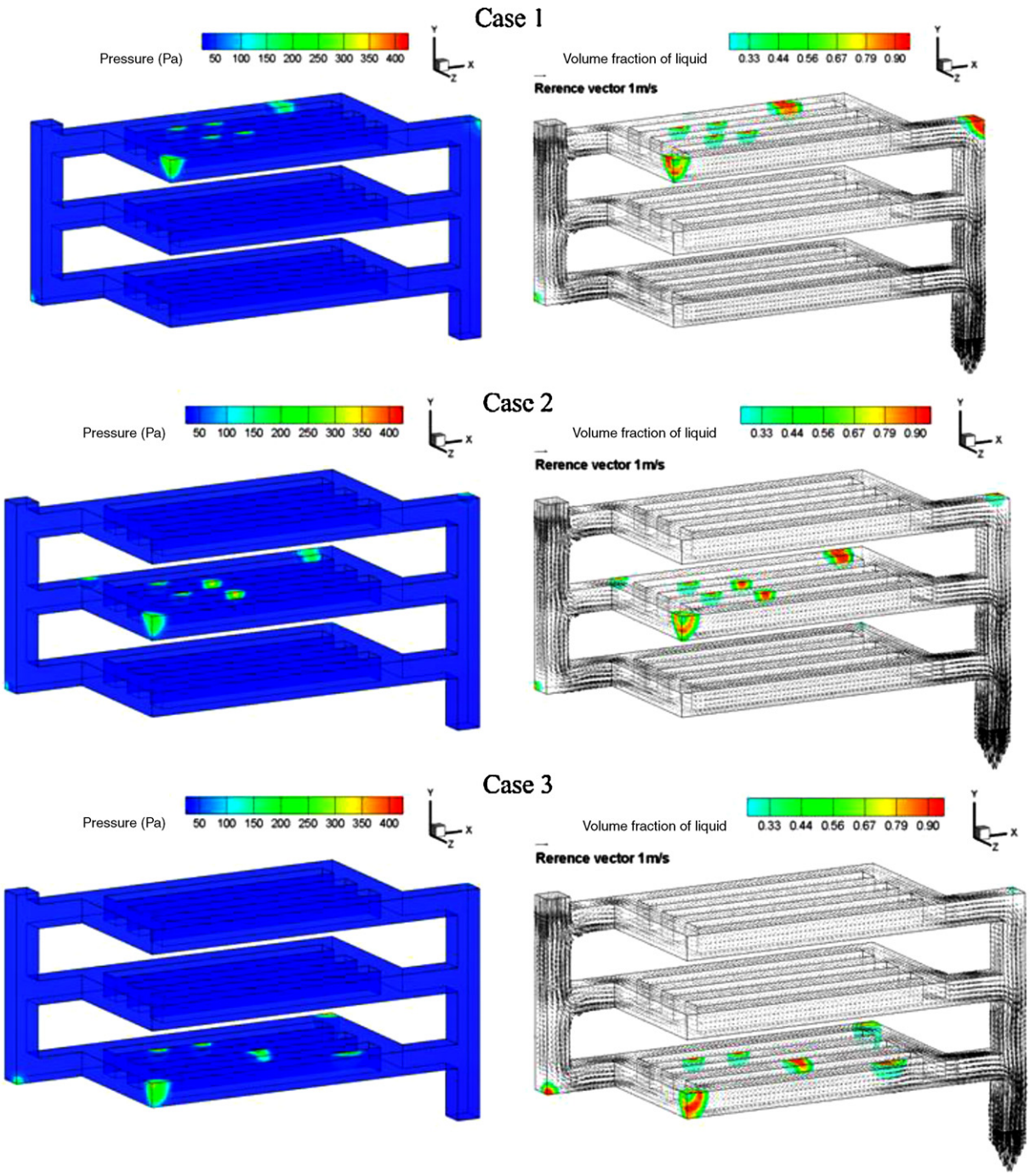

Fig. 3. Pressure and velocity distributions in the air channel of three cases at $t = 3$ s.

the saturated pressure is a function of temperature, describing as follows:

$$P_{sat} = 101325 \times 10^{(-2.1794+0.02953\times(T-273.17)-9.1837*10^{-5}\times(T-273.17)^2+1.4454\times10^{-7}\times(T-273.17)^3)} \quad (17)$$

In addition, water may diffuse through the membrane due to the concentration gradient driven mechanism according to the Fick's law [26]. Hence, the net water flux through the membrane results in a water balance between the electro-osmotic drag and back diffusion as follows:

$$J_w = J_w^{os} + J_w^{diff} = n_d \frac{M_{H_2O}}{F}\vec{I} - D_{w,m}\nabla(\rho Y_w) \quad (18)$$

In Eq. (12), the membrane water diffusivity were experimentally measured by Motupally et al. [27]:

$$D_{w,m} = \begin{cases} 3.10\times10^{-3}\ \lambda(-1+e^{0.28\lambda})\exp\left(\dfrac{-2436}{T}\right) & 0<\lambda\le 3 \\ 4.17\times10^{-4}(1+161e^{-\lambda})\exp\left(\dfrac{-2436}{T}\right) & 3<\lambda<17 \end{cases} \quad (19)$$

The other source term due to phase change is also seen in water transport equation (12). Once an amount of water is transferred from water vapor to liquid water or vice versa, this amount is taken into account as the generation (liquid to vapor phase) or as the consumption (vapor to liquid phase) in the water transport source term. The phase change mechanism in this model is examined by thermodynamic equilibrium condition $\Delta P = P_{wv} - P_{sat}$ to

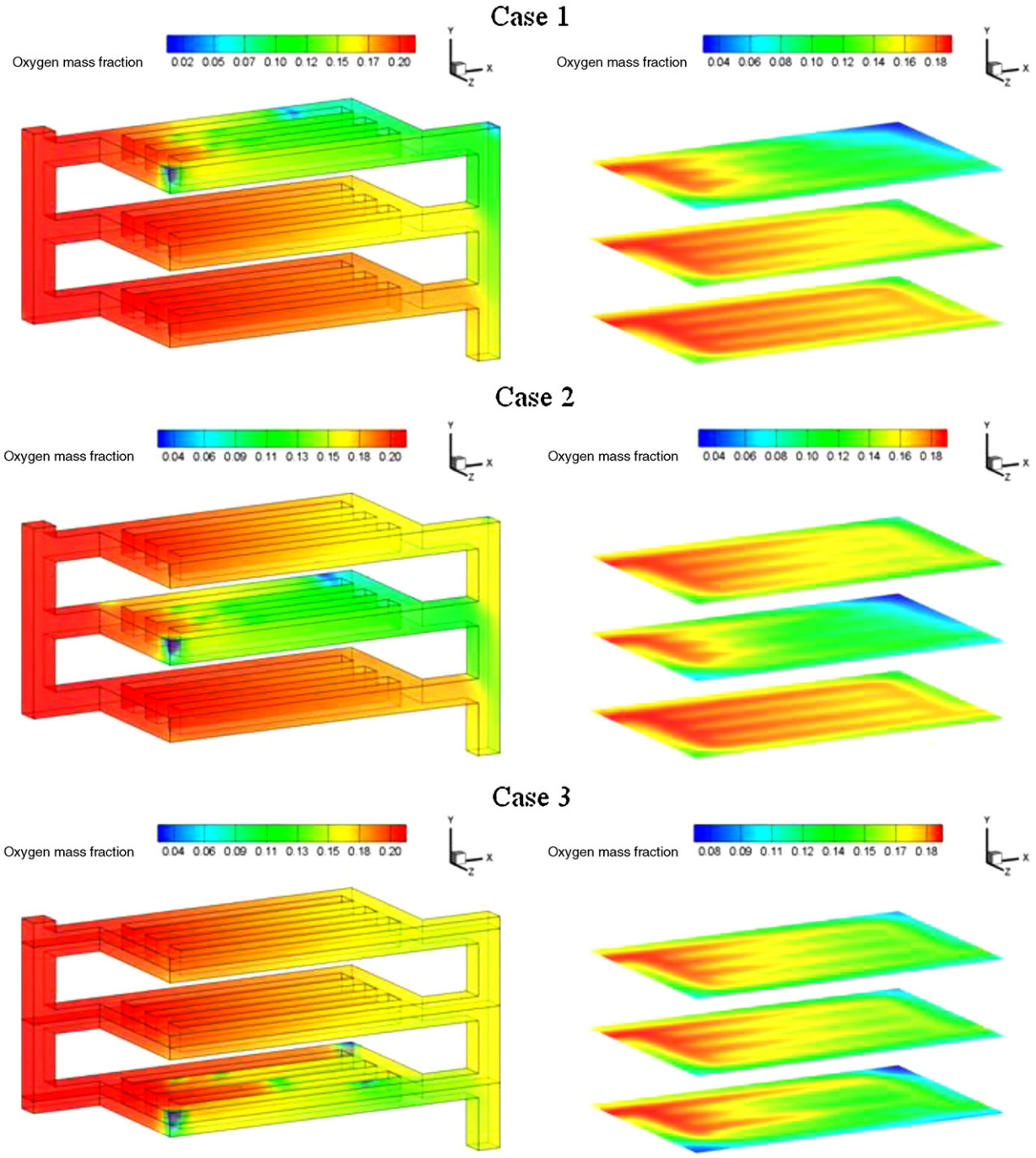

Fig. 4. Oxygen distribution in the cathode channel and catalyst layer of three cases at $t = 3$ s.

determine the phase change rate r_w:

$$r_w = \begin{cases} c_r(1-s_l)\dfrac{P_{wv}-P_{sat}}{RT}M_{H_2O} & P_{wv} \geq P_{sat} \\ -c_r s_l \rho_l & P_{wv} < P_{sat} \end{cases} \quad (20)$$

In Eq. (20), the phase change rate is positive as the phase change is condensation and the phase change rate is negative as evaporation occurs. The phase change rate also plays an important role in determining the mass and energy transfers in PEMFC since it appears in the source terms of mass, species and energy equations as shown in Table 1.

The current transport of electrons through the solid phase and protons through the membrane phase was conducted by conservation equations of charges:

$$\nabla \cdot (\sigma_s \nabla \phi_s) = S_{es} \quad (21)$$

$$\nabla \cdot (\sigma_m \nabla \phi_m) = S_{em} \quad (22)$$

The volumetric transfer currents are driven by the activation overpotential η, which is the potential difference between solid and membrane phases. The electronic conductivity of solid materials is constant, depending on the material property and the protonic conductivity of Nafion membrane used in the model is calculated by using the formulation described by Springer et al. [2]:

$$\sigma_m = \varepsilon(0.514\lambda - 0.326)e^{1268(1/303 - 1/T)} \quad (23)$$

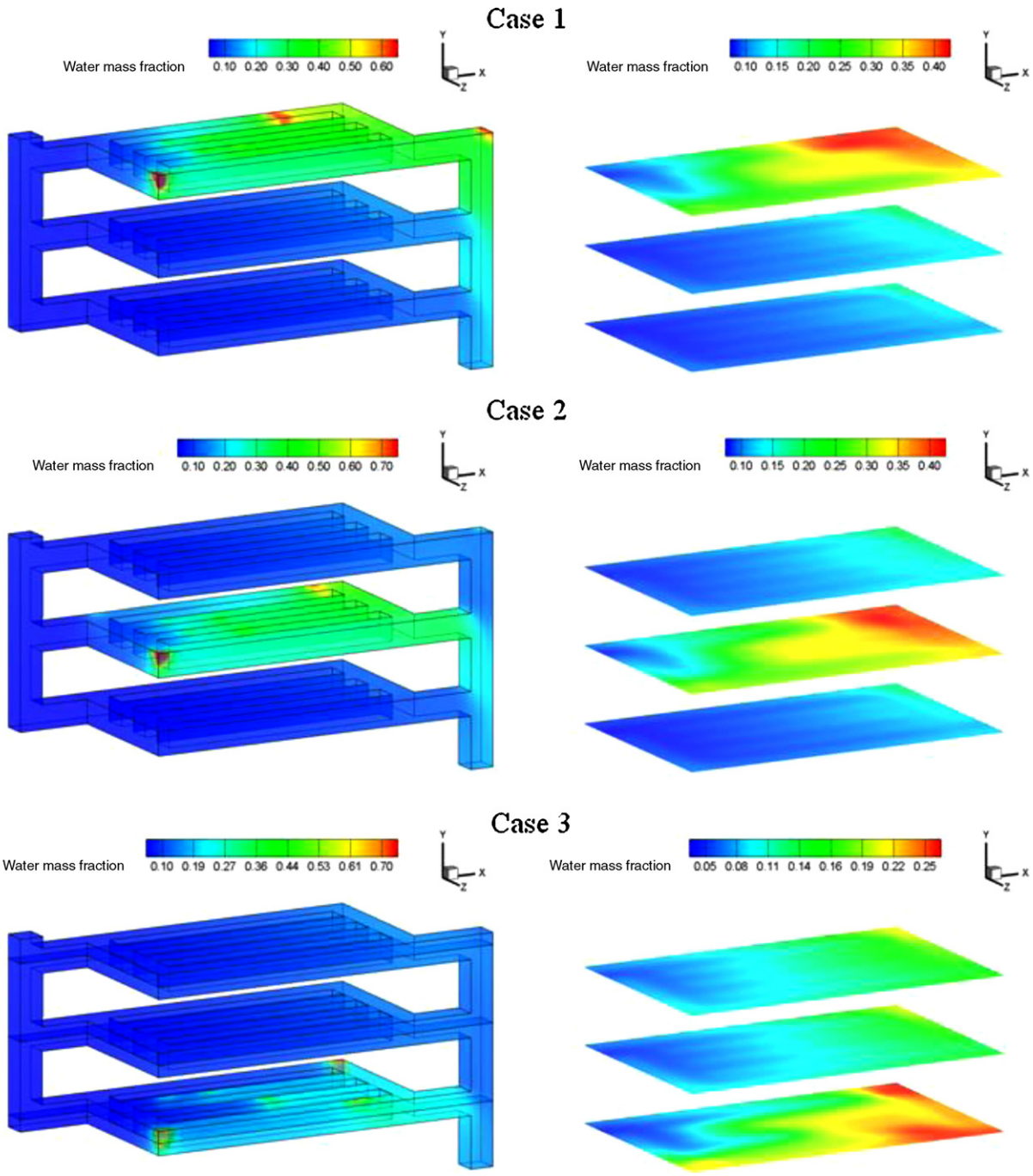

Fig. 5. Water distribution in the cathode channel and catalyst layer of three cases at $t = 3$ s.

The source terms for the solid phase and the membrane phase represent the electron and proton generation, respectively, and are determined by Butler–Volmer equation [28]:

$$R_{an} = R_{an}^{ref}\left(\frac{C_{H_2}}{C_{H_2}^{ref}}\right)^{\gamma_{an}}\left[\exp\left(\frac{\alpha_{an,an}F\eta_{an}}{RT}\right) - \exp\left(-\frac{\alpha_{cat,an}F\eta_{cat}}{RT}\right)\right] \tag{24}$$

$$R_{cat} = R_{cat}^{ref}\left(\frac{C_{O_2}}{C_{O_2}^{ref}}\right)^{\gamma_{cat}}\left[\exp\left(-\frac{\alpha_{cat,cat}F\eta_{cat}}{RT}\right) - \exp\left(\frac{\alpha_{an,cat}F\eta_{an}}{RT}\right)\right] \tag{25}$$

The cell potential is the difference between the cathode and anode solid phase at the terminal collectors (two ends of the cell collectors which are connected to the external electric circuit). Following the conservation of charge, the total current of either electrons or protons exiting from the anode catalyst layer must be equal to the total current entering the cathode catalyst layer and must be equal to the total current caused by the proton movement through the membrane:

$$\sum_{V_{an}} R_{an}\,dV = \sum_{V_{cat}} R_{cat}\,dV \tag{26}$$

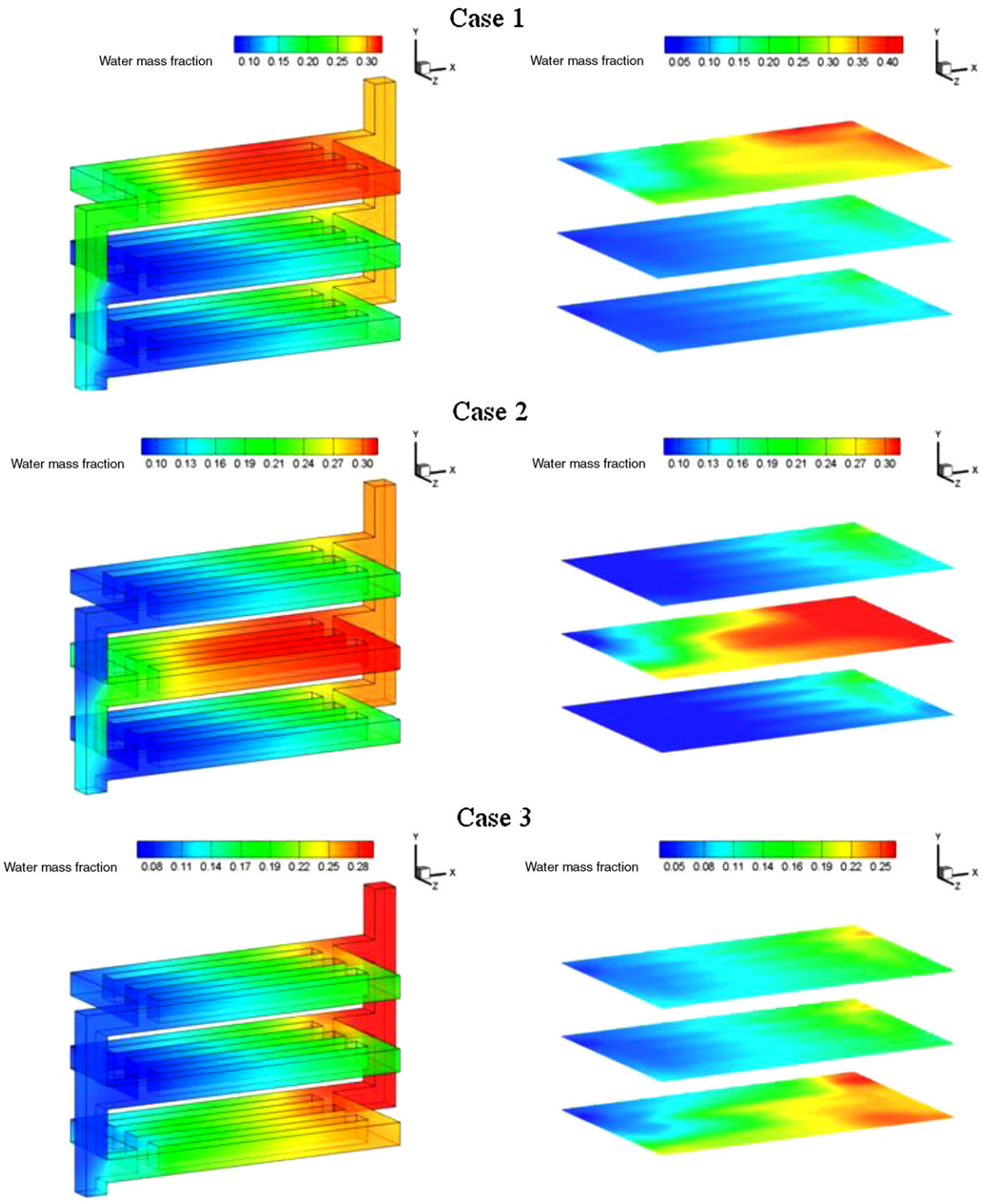

Fig. 6. Water distribution in the anode channel and catalyst layer of three cases at $t = 3$ s.

2.3. Boundary conditions

For the flow inlet boundary, the inlet flow rates of gas species are predetermined based on the reference current density $I_{ref} = 1$ A/cm^2 and excess coefficients ω_{H_2} and ω_{O_2}:

$$\dot{m}_{H_2,in} = U_{H_2,in}\rho_{H_2}A_{in} = \omega_{H_2}M_{H_2}\frac{I_{ref}\sum_i A_{surf}}{2F} \quad (27)$$

$$\dot{m}_{O_2,in} = U_{O_2,in}\rho_{O_2}A_{in} = \omega_{O_2}M_{O_2}\frac{I_{ref}\sum_i A_{surf}}{4F} \quad (28)$$

where $\sum_i A_{surf}$ is total of the active reaction areas of single cells in the stack. The inlet temperature and mass fractions of species are also determined as the operating condition of the fuel cell stack, as given in Table 2.

For the flow outlet boundary, the fully developed flow condition and no-flux conditions are applied for velocity and temperature

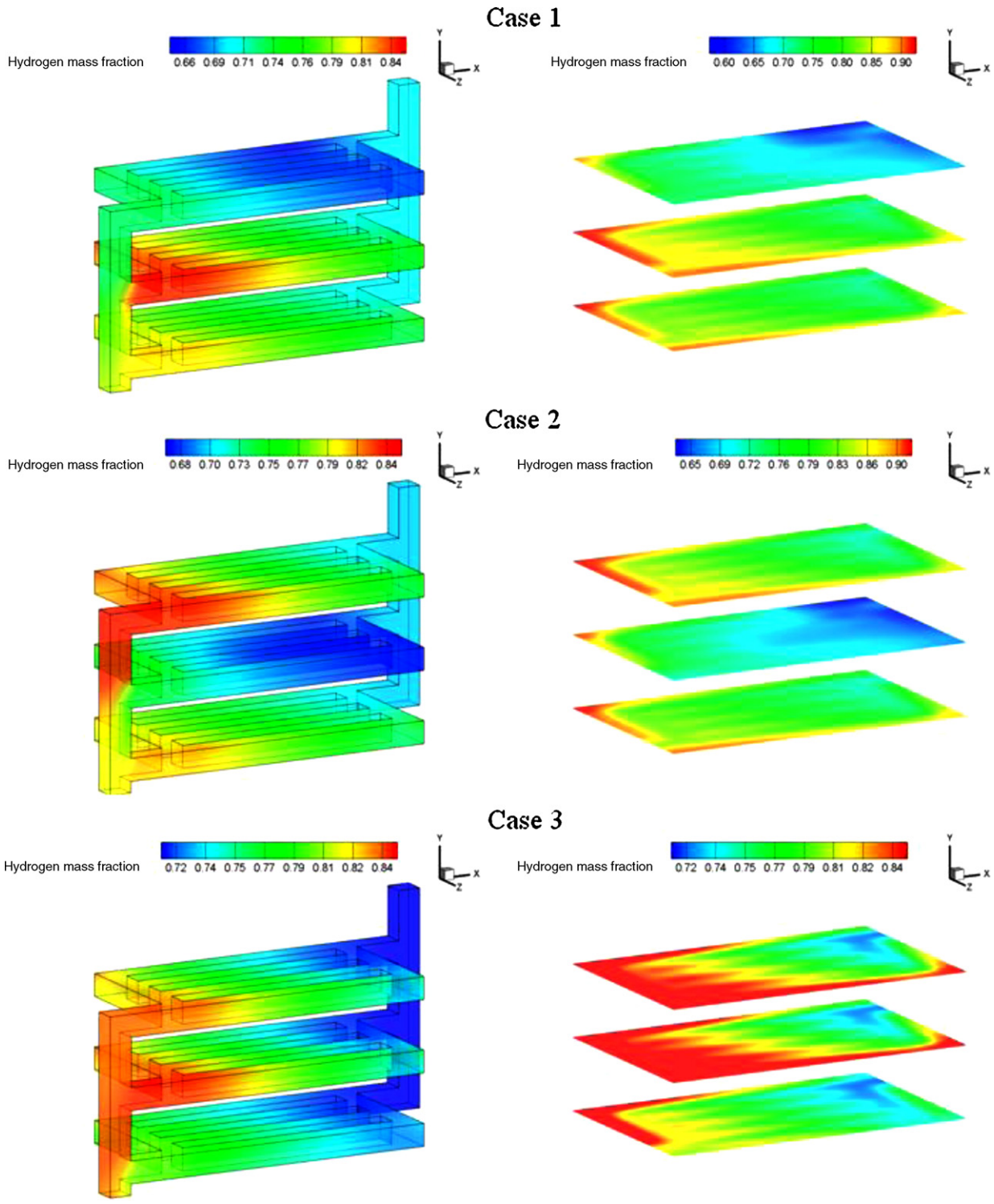

Fig. 7. Hydrogen distribution in the anode channel and catalyst layer of three cases at $t = 3$ s.

field, and concentrations of gas species:

$$\frac{\partial \vec{u}}{\partial n} = 0, \qquad \frac{\partial T}{\partial n} = 0 \quad \text{and} \quad \frac{\partial Y_i}{\partial n} = 0 \tag{29}$$

For the anode and cathode terminals of the stack where the anode and cathode collectors were, respectively, connected to the external electric circuit (electric load), the boundary conditions for phase potentials on the surface are determined as follows:

$$\phi_{s,an} = 0, \qquad \left.\frac{\partial \phi_m}{\partial n}\right|_{an} = 0 \tag{30}$$

$$\phi_{s,cat} = V_{stack}, \qquad \left.\frac{\partial \phi_m}{\partial n}\right|_{cat} = 0 \tag{31}$$

Note that the sum of the single cells voltage is the stack voltage set in the cathode terminal.

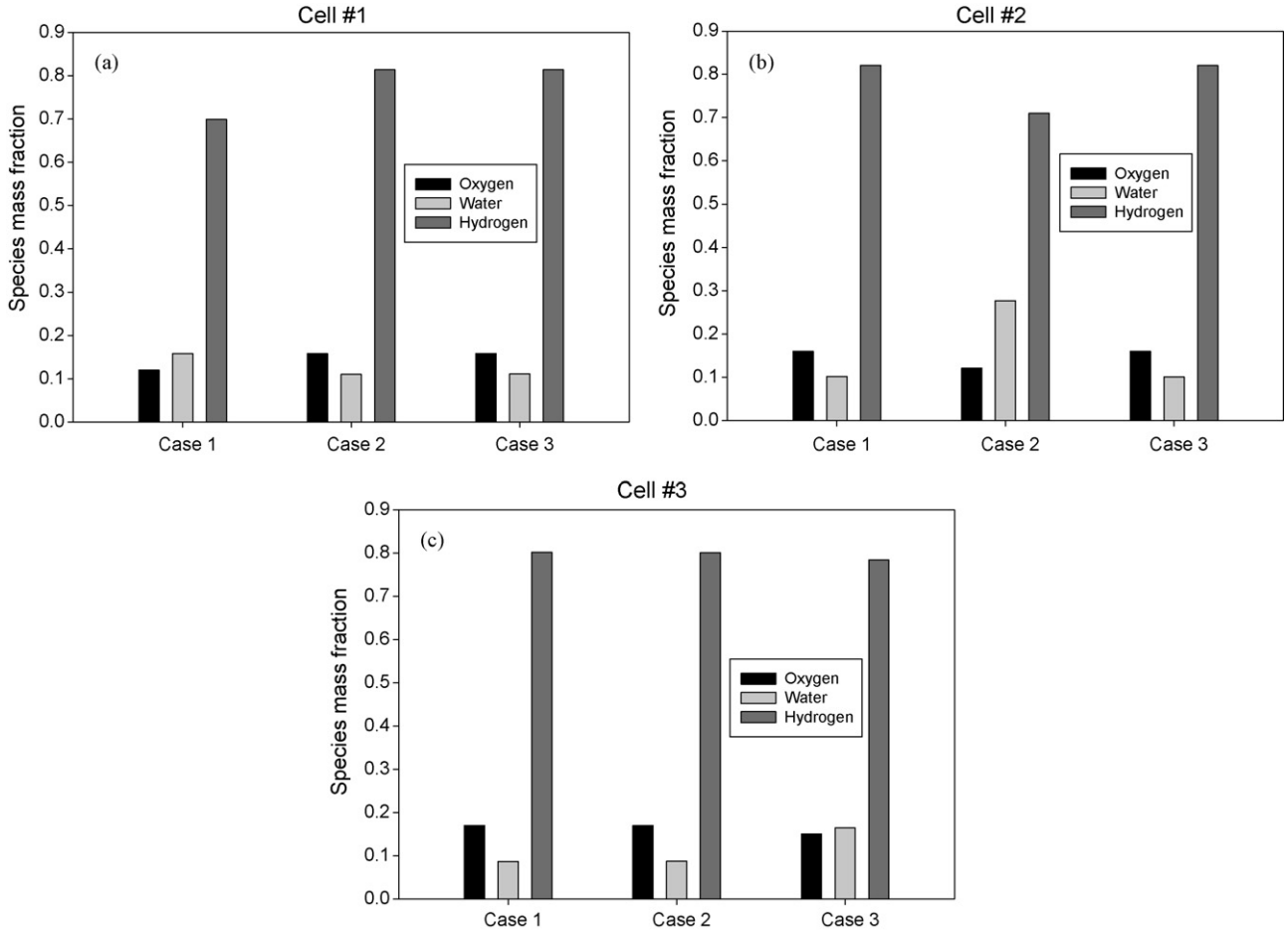

Fig. 8. Average mass fraction distributions of species in three single cells at $t = 3$ s of three cases.

Since the unified-domain approach was employed to develop this model, it is not necessary to declare the internal boundary conditions for the internal interfaces. However, for the external walls except the anode and cathode terminals, the zero values are applied to all velocity components and no-flux condition are used to describe for variables of gas species, temperature and potential fields:

$$\vec{u}_i = 0, \qquad \frac{\partial \phi_s}{\partial n} = 0; \qquad \frac{\partial \phi_m}{\partial n} = 0 \tag{32}$$

The fuel cell might be overheating during its operation due to the thermal amount generated from the reactions and electric resistance. To overcome the lack of cooling channels that are used to control the temperature, the forced convection is applied onto the external walls of the stack. The heat generation rate from the stack is assumed to be a product of the total current $\bar{I}$ and potential loss as follows [29]:

$$\dot{Q}_{generation} = \bar{I}(1.25 - V_{cell}) \tag{33}$$

Thus, to make sure that the forced convection dissipates the generation heat, the thermal condition for the external boundary is required:

$$\dot{Q}_{convection} = \dot{Q}_{generated} \tag{34}$$

And the heat convective coefficient set for cooling the external walls then can be determined:

$$h = \frac{\bar{I}(1.25 - V_{cell})}{A_{wall}(T_{wall} - T_{\infty})} \tag{35}$$

3. Volume-of-fluid (VOF) algorithm and numerical procedure

3.1. Volume-of-fluid algorithm

To examine the gas–liquid phases transport in the PEMFC stack, the VOF technique has been selected to track immiscible interfaces between gas phase and liquid phase in the channels and the voids of the porous media. The VOF method, which uses the static grid to locate the fluids, is very popular for the simulation the multi-fluid flow problems with significant changes of the interface topology. The purpose of using VOF technique to PEMFC model is to track the motion and shape of gas mixture-liquid water interface in a flow field, thus investigating the water liquid transport in a fuel cell stack and its effects on the cell performance. The principle steps in a VOF method are reconstructed interface geometry and time integration algorithms. The VOF geometric reconstruction scheme is generally divided into two parts: a reconstruction step and a propagation step. In this model, the geometric reconstruction piecewise linear interface construction (PLIC) scheme was chosen due to its accuracy and applicability for general unstructured meshes, compared to other methods such as the donor–acceptor, Euler explicit, and implicit schemes. More details of the VOF algorithm used in Fluent® 6.3 CFD software can be seen in Ref. [24].

3.2. Computational domain and numerical procedure

The computational domain contains 399,650 hexahedral grid cells and is implemented by Gambit® 2.3 mesh generation soft-

ware as shown in Fig. 1. The volume control approach implemented in fluent solver is used to solve the coupled set of governing and constituent equations. The physical transport, source terms and boundary conditions are customized by our own user-defined-functions (UDFs) written in C language. To obtain the numerical results with high accuracy and precision, the double precision solver is chosen and the convergence criteria for species, energy and charge transports are set to be approximate 10^{-5}.

4. Results and discussion

Liquid droplet injection is an effective way to examine the effects of liquid transport on flow field behavior, species and charge transport. Since the computation of VOF method is temporally expensive, it takes few months to have an Intel® Core2-Quad PC running in tens of seconds of flow time to obtain a little amount of liquid droplets in the fuel cell. In this stack model, therefore, the droplets are added into the cathode channel of each individual cell at $t = 1$ s. As the time progresses, the numerical results are continuously simulated. To investigate the flow and transport behaviors in the stack, the results at $t = 3$ s are described and analyzed. Geometrical properties and physical parameters of the stack are listed in Table 2.

4.1. Liquid water distribution in the air channel of three cases at different instants

The three different cases corresponding to different locations of droplet addition are listed in Table 3. Fig. 2a shows the location of droplets at the initial time $t = 0$ s. Fig. 2b–d shows the liquid droplet distributions in the cathode flow channel of three single cells in the stack at time instants of 2, 3 and 4 s. The information about droplet behaviors at 3 s in a fuel cell stack at different single cells is examined to facilitate the analysis on the effects of liquid water to fluid flow and species distribution characteristics of the single cells in the stack.

4.2. Pressure and flow field distribution in the cathode channel of three cases at t = 3 s

Fig. 3 shows the distribution of pressure and flow field under the presence of liquid water in the channels in different cells. It can be observed that liquid droplets present in a channel of a certain cell will locally cause an uneven distribution of pressure and flow field in this channel. First, one can notice that the pressure drop across the surface of droplets is relatively high compared with the pressure difference in the channel. Second, in the case of straight-parallel channel, the block of droplets in a channel works as a resistance, causing a decrease of the velocity of gas flow through the channel.

Regarding the straight-parallel channel, the numerical results show that this design ensures the distribution of flow field and pressure drop are more uniform than other channel designs (as shown in Fig. 3: there is no significant change of flow velocity under the presence of liquid droplets). However, the straight-parallel channel may not be applicable to remove the liquid droplets from the channel as observed in Fig. 3.

4.3. Species transport distribution in the channels and catalyst layers of three cases at t = 3 s

In Figs. 4 and 5, the mass fraction distributions of oxygen and water in the cathode channel and catalyst layer of three cases are shown. The species distributions illustrate that the oxygen transport is hindered by liquid droplets present in the channel. As shown in Case 1, at the top of the cathode channel (of cell 1) a number of droplets degrades the mass transport of oxygen, leading to a low concentration of oxygen when it is compared with the oxygen concentrations at the same channel in Cases 2 and 3. Similar to Case 1, the species distributions in Cases 2 and 3 show low concentration of oxygen at the middle channel and the bottom channel where the liquid water is present. Certainly, a low oxygen distribution in the channel results in a small amount of oxygen concentrated in the catalyst layer in the same cell. It also causes a low current density distribution when the cell contains a large amount of liquid water, since the concentration distribution of oxygen is proportional to the reaction rate.

Because the liquid water and water vapor are considered as the same species, the water distribution shown in Fig. 5 denotes mass fraction distribution of water, regardless of liquid or vapor phase. Although the phase change of water is taken into account in this model, the amount of water in terms of liquid water and water vapor at a location is unchanged. Thus, once liquid water is located in the channel of a certain single cell, the water distribution becomes high, especially at the locations where the liquid droplets are present.

Fig. 6 depicts the water fraction distributions in the anode channel and catalyst layer of three cases. Note that the liquid water is not present in the anode by adding droplets from $t = 0$ s as in the cathode, the species mass fractions in the anode, however, are still affected by the distributions of reactant gas in the cathode due to water transport through the membrane. Let us explain this comment according to Case 1 shown in Fig. 6 for water mass fraction. One can easily see that the water mass fraction in the anode channel of the cell 1 is higher than that in the cell 2 and cell 3. Corresponding to this distribution, the water mass fraction in the cathode channel of the cell 1 is also higher than that in other cells as described above. Thus, it can be concluded that the presence of liquid water in the cathode not only affects the water distribution in the cathode itself, but also influences the water distribution in the anode by water transport mechanism in a single cell. Moreover, as a consequence, the hydrogen fraction distribution is also altered corresponding to water distribution in the anode since the total mass fractions of hydrogen and water is unity in the anode, as shown in Fig. 7.

To quantitatively examine the effects of liquid water on the distributions of species in each single cell in three cases, Fig. 8 shows the distributions of oxygen and water in the cathode catalyst layer, and the distribution of hydrogen in the anode catalyst layer of the same cell at $t = 3$ s. Fig. 8a shows the species distributions in cell #1, Fig. 8b shows the species distributions in cell #2 and Fig. 8c shows the species distributions in cell #3 of three different cases, respectively. It can be seen that in the single cell with the presence of liquid droplets, the distributions of oxygen and hydrogen are lower and the distribution of water is higher than the distributions in other cells. Since the concentration loss is influenced by the mass transport of the reactant gases in the catalyst layers, the low distributions of species in the flooding cell certainly degrade the performance of this cell. This effect can also be described in current density distributions of single cells in the stack.

4.4. Potential and current density distributions in the stack of three cases at t = 3 s

With a fixed cell voltage of 1.8 V applied on the fuel cell stack, the voltage and current density distributed in each single cell and the stack are calculated in the transient state. Here the current density distributions in the membrane of each single cell at $t = 3$ s are presented to investigate the effects of liquid water on the fuel cell performance. The uneven distribution of flow field and species concentration, as analyzed above, that is caused by the presence of liquid is the main reason to cause uneven current density distribution. As shown in Fig. 9, a degradation of current density occurs only at the cell containing the liquid water. This mechanism of the cur-

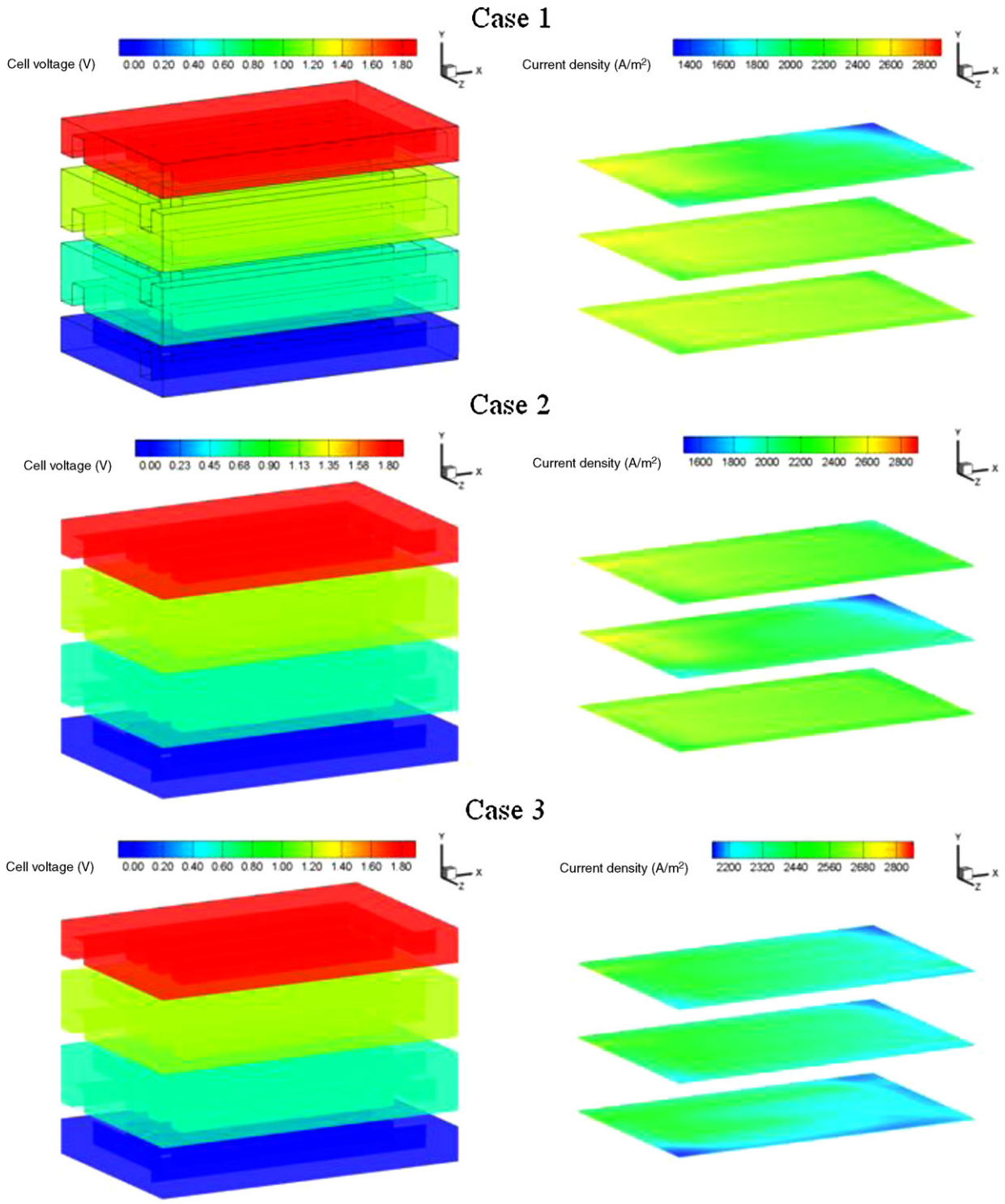

Fig. 9. Potential and current density distributions in each single cell of three cases at $t = 3$ s.

rent density degradation was explained in details in our previous studies [13,15] and hence, it is briefly mentioned in the stack model to illustrate the effects of liquid water on the PEMFC stack performance. In Fig. 9, the current density distribution in the flooding cell looks smaller than in other cells containing no liquid water. Again, this phenomenon demonstrates that the current density generated from a flooding single cell is degraded due to the presence of liquid water. Although the average current densities in the cells without containing liquid water are temporarily higher, these values will be eventually reduced to be the same with the average current density in the flooding cell due to charge conservation in series connection. The temporal difference among these values of current density is due to the fact the numerical results are obtained at a certain time in the transient state. When the state is steady, the value of current density of the fuel cell stack is equal to the value of current density of the flooding single cell. In addition, the voltages of each cell and the whole stack also achieved from the numerical model. Fig. 9 shows that the values of cell potential are approximately 0.6 V for every cell in the stack with the stack potential valued at 1.8 V.

5. Conclusions

In this study, a three-dimensional, multi-phase, PEMFC model coupled with VOF algorithm is applied into a PEMFC stack. The numerical simulation has been successfully developed to customize the governing and relative equations and their source terms in order to describe all physical and electrochemical phenomena in a PEMFC stack. The numerical results show that the model can predict a number of important parameters such as flow field, species concentrations, temperature, voltage and current density distributions in all single cells of the stack under various operating and design parameters. The PEMFC stack model also considers the presence of liquid water inside the manifold, channels and porous media as well. The numerical results from three cases for different liquid droplet locations in different single cells indicate that presenting liquid droplets in the stack is an effective way to examine the flooding phenomenon in single cells. It is shown that the distributions of reactant gases in the flooding cell are lower than in the other cells containing no liquid water. The local flooding in a certain single cell leads to degradation of the mass transport, resulting in a decrease in the current density distribution. When the performance of a flooding cell is diminished due to presence of liquid water, it will significantly affect the whole stack performance since the values of average current density of all single cells must be identical in series connection fuel cell stack. Again, the combination of a general model of PEMFC and VOF method is a powerful and effective tool for PEMFC stack design and simulation to investigate the fluid dynamics, mass transport, flooding phenomenon and the effects of liquid water on the stack performance.

Acknowledgments

The authors are grateful to the Auto21™ Networks of Centers of Excellence (Grant D303-DFC), the Natural Sciences and Engineering Research Council of Canada (NSERC), the Canada Foundation for Innovation (CFI), the Ontario Innovation Trust (OIT), and the University of Windsor for the support of this work.

References

[1] D.M. Bernardi, M.W. Verbrugge, J. Electrochem. Soc. 139 (1992) 2477.
[2] T. Springer, T. Zawodzinski, S. Gosttesfeld, J. Electrochem. Soc. 139 (1992) 2477.
[3] S. Um, C.Y. Wang, K.S. Chen, J. Electrochem. Soc. 147 (2000) 4485.
[4] S. Dutta, S. Simpalee, J.W. Van Zee, J. Appl. Electrochem. 30 (2000) 135.
[5] S. Ge, B. Yi, J. Power Sources 124 (2003) 1.
[6] P.T. Nguyen, T. Berning, N. Djilali, J. Power Sources 130 (2004) 149.
[7] W. Huang, B. Zhou, A. Sobiesiak, Int. J. Energy Res. 29 (2005) 1051.
[8] L. You, H. Liu, J. Power Sources 155 (2006) 219.
[9] W. Huang, B. Zhou, A. Sobesiak, J. Electrochem. Soc. 1945 (2006) 153.
[10] G. Lin, T.V. Nguyen, J. Electrochem. Soc. 153 (2006) A372.
[11] M. M. Vynnycky, Appl. Math. Comput. 189 (2007) 1560.
[12] Y. Wang, S. Basu, C.Y. Wang, J. Power Sources 179 (2008) 603–617.
[13] A.D. Le, B. Zhou, J. Power Sources 182 (2008) 197–222.
[14] A.A. Shah, T.R. Ralph, F.C. Walsh, J. Electrochem. Soc. 156 (4) (2009) B465.
[15] A.D. Le, B. Zhou, Electrochim. Acta 54 (2009) 2137.
[16] Y. Shan, S.Y. Choe, S.H. Choi, J. Power Sources 165 (2007) 196.
[17] Z. Liu, Z. Mao, C. Wang, W. Zhuge, Y. Zhang, J. Power Sources 160 (2006) 1111.
[18] C.H. Chen, S.P. Jung, S.C. Yen, J. Power Sources 173 (2007) 249.
[19] R. Mustata, L. Valino, F. Barreras, M.I. Gil, A. Lozano, J. Power Sources 192 (2009) 185.
[20] Y. Zhang, A. Mawardi, R. Pitchumani, J. Power Sources 173 (2007) 264.
[21] S. Shimpalee, M. Ohashi, J.W. Van Zee, C. Ziegler, C. Stoeckmann, C. Sadeler, C. Hebling, Electrochim. Acta 54 (10) (2009) 2899.
[22] K. Jiao, B. Zhou, P. Quan, J. Power Sources 154 (2006) 124.
[23] G. Karimi, F. Jafapour, X. Li, J. Power Sources 187 (2009) 156.
[24] Fluent® 6. 3 Manual, Fluent Inc., 2006.
[25] R. O'Hayre, S.W. Cha, W. Colella, F.B. Prinz, Fuel Cell Fundamentals, John Wiley & Sons, New York, 2006.
[26] R.B. Bird, Transport Phenomena, 2nd ed., John Wiley & Sons, 2001, pp 514-515.
[27] S. Motupally, A.J. Becker, J.M. Weidner, J. Electrochem. Soc. 147 (2000) 3171.
[28] A.J. Bard, R.L. Faulkner, Electrochemical Methods: Fundamentals and Applications, J. Wiley & Sons, 2001, pp. 92–107.
[29] J. Larminie, A. Dicks, Fuel Cell Systems Explained, 2nd ed., John Wiley & Sons, England, 2003, p. 400.